HHS Public Access

Author manuscript

Cell. Author manuscript; available in PMC 2024 March 02.

Published in final edited form as:

Cell. 2023 March 02; 186(5): 1039–1049.e17. doi:10.1016/j.cell.2023.01.013.

A molecular device for the redox quality control of GroEL/ES substrates

Emile Dupuy[1,2,3], **Sander Egbert Van der Verren**[3,4,5], **Jiusheng Lin**[6], **Mark Alan Wilson**[6], **Alix Vincent Dachsbeck**[1,2], **Felipe Viela**[7], **Emmanuelle Latour**[1,2], **Alexandra Gennaris**[1,2], **Didier Vertommen**[2], **Yves Frédéric Dufrêne**[7], **Bogdan Iuliu Iorga**[1,2,8], **Camille Véronique Goemans**[1,2,9,*], **Han Remaut**[4,5,*], **Jean-François Collet**[1,2,10,*]

[1]WELBIO, Avenue Hippocrate 75, 1200 Brussels, Belgium

[2]de Duve Institute, Université catholique de Louvain, Avenue Hippocrate 75, 1200 Brussels, Belgium

[3]These authors contributed equally

[4]Structural Biology Brussels, Vrije Universiteit Brussel, 1050 Brussels, Belgium

[5]Structural and Molecular Microbiology, Structural Biology Research Center, VIB, 1050 Brussels, Belgium

[6]Department of Biochemistry and the Redox Biology Center, University of Nebraska, Lincoln, NE 68588, USA

[7]Louvain Institute of Biomolecular Science and Technology, Université Catholique de Louvain, Croix du Sud 4-5, 1348 Louvain-la-neuve, Belgium

[8]Université Paris-Saclay, CNRS UPR 2301, Institut de Chimie des Substances Naturelles, 91198 Gif-sur-Yvette, France

[9]European Molecular Biology Laboratory, Meyerhofstrasse 1, 69117 Heidelberg, Germany

[10]Lead contact

SUMMARY

Hsp60 chaperonins and their Hsp10 cofactors assist protein folding in all living cells, constituting the paradigmatic example of molecular chaperones. Despite extensive investigations of their

*Corresponding authors: Jean-François Collet (jfcollet@uclouvain.be), Camille Goemans (camille.goemans@embl.de), Han Remaut (han.remaut@vub.be).

AUTHOR CONTRIBUTIONS

Writing: JFC, SEVdV, ED, HR, and CVG. Conceptualization: CVG, ED, HR, and JFC. Investigation, strain construction, construct cloning: ED, CVG, AVD, AG, SEVdV, JL, MAW, EL, YFD, and FV. Identification and AlphaFold modeling of CnoX mammalian homologs: BII. Mass spectrometry: DV. Data analysis and interpretation: ED, SEVdV, CVG, HR, JL, MAW, YFD, FV, and JFC. All authors discussed the results and commented on the manuscript.

DECLARATION OF INTERESTS

The authors declare no competing interests.

structure and mechanism, crucial questions regarding how these chaperonins promote folding remain unsolved. Here, we report that the bacterial Hsp60 chaperonin GroEL forms a stable, functionally relevant complex with the chaperedoxin CnoX, a protein combining a chaperone and a redox function. Binding of GroES (Hsp10 cofactor) to GroEL induces CnoX release. Cryo-electron microscopy provided crucial structural information on the GroEL-CnoX complex, showing that CnoX binds GroEL outside the substrate-binding site via a highly conserved C-terminal α-helix. Furthermore, we identified complexes in which CnoX, bound to GroEL, forms mixed disulfides with GroEL substrates, indicating that CnoX likely functions as a redox quality-control plugin for GroEL. Proteins sharing structural features with CnoX exist in eukaryotes, suggesting that Hsp60 molecular plugins have been conserved through evolution.

Graphical Abstract

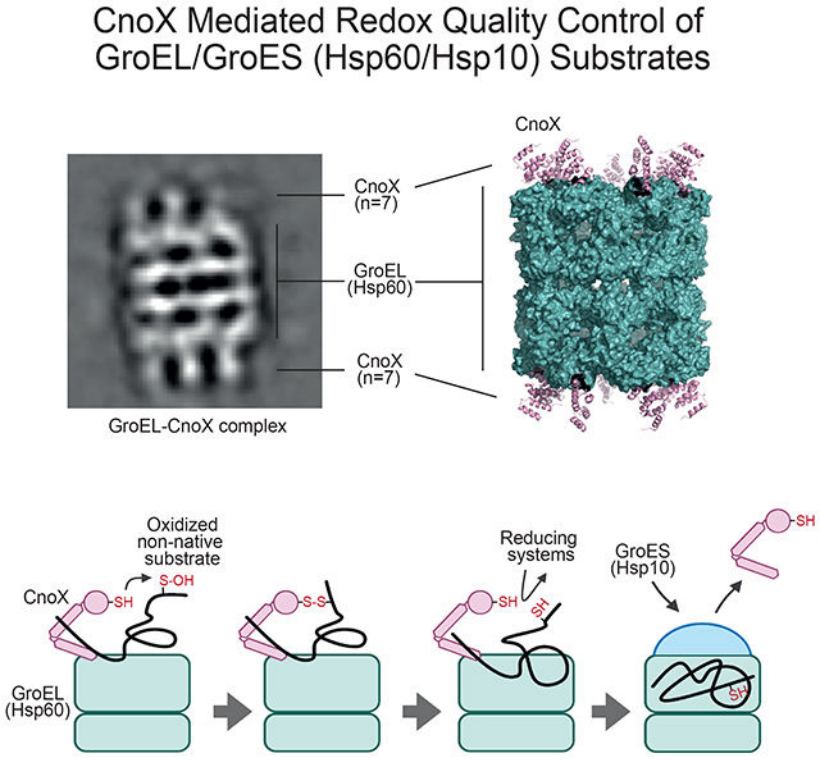

In Brief:

CnoX is a redox quality-control molecular plugin for an evolutionarily conserved Hsp60 chaperonin complex crucial for protein folding in all living cells

Keywords

Protein folding; chaperones; redox; proteostasis; TPR; thioredoxin; chaperonin

INTRODUCTION

Following synthesis as linear amino-acid chains, proteins must fold to unique three-dimensional (3D) structures to become functional. Seminal work from Anfinsen demonstrated that the information required for a polypeptide to reach its native conformation is contained in its primary sequence.[1] For most small proteins, folding to the native state is a spontaneous process that takes less than a few milliseconds.[2] For larger proteins with multiple domains, however, the path to the native conformation is more tortuous and potentially hazardous. For these proteins, stable intermediates can form, slowing the folding process and potentially leading to aggregation and/or degradation.[3] To deal with this problem, living cells express a network of chaperones that help complex proteins to fold efficiently.[4]

The Hsp60 chaperonins are a unique class of chaperones that are essential in all domains of life and prevent unproductive interactions within and between polypeptides using adenosine triphosphate (ATP)-regulated cycles.[5–7] Chaperonins stand out in the proteostasis network, as they form a complex tetradecameric structure encompassing a large cylindrical cage consisting of two seven-membered rings stacked back to back (Figure S1A).[8,9] Each Hsp60 subunit consists of an ATP-binding equatorial domain, an intermediate domain, and an apical substrate-binding domain (Figure S1A).[10] Hsp60 cooperates with Hsp10 [11], which forms a heptameric dome-like structure (Figure S1A).[12] In the presence of nucleotides, Hsp10 associates with the apical domain of Hsp60, binding as a lid covering the ends of the ring and forming a folding chamber[13] referred to as the “Anfinsen cage.” Binding of Hsp10 to a substrate-loaded Hsp60 results in displacement of the substrate into the chamber, where it can fold protected from outside interactions.[14,15]

The mechanism by which chaperonins assist substrate proteins in navigating the folding landscape to their native state is relatively well understood. Although this is particularly true for the *Escherichia coli* Hsp60 chaperonin GroEL and GroES, its Hsp10 cofactor, several crucial questions remain unsolved. For instance, whether the GroEL-GroES nanomachine actively promotes folding or serves only as a passive folding cage remains controversial.[7] It is also unknown why some polypeptides are highly dependent on GroEL-GroES for folding whereas homologous proteins with a similar structure fold independently of the chaperonin.[7] Thus, further investigation is required to elucidate the sorting signals that recruit substrate proteins to the Hsp60 folding cage. Moreover, recent results have indicated that the integration of GroEL-GroES in the cellular proteostasis network also needs further exploration. Indeed, the identification of CnoX as the first chaperone capable of transferring its substrates to GroEL-GroES for active refolding[16,17] suggests that functional links between GroEL-GroES and accessory folding factors remain to be discovered. The extreme complexity of the GroEL-GroES molecular machine, its essential role in cell survival, and redundancy in the bacterial proteostasis system have slowed progress in the field, highlighting the need for new investigation approaches and experimental strategies.

Here, we sought to explore the details of the newly reported CnoX-GroEL functional relationship[16,17], with the aim of revealing unsuspected features of the GroEL-GroES system. CnoX consists of a redox-active N-terminal thioredoxin domain and a C-terminal

tetratricopeptide (TPR) domain (Figure S1B)[18], a fold often involved in protein–protein interactions. CnoX is a "chaperedoxin," meaning that it combines a redox-protective function, by which it prevents irreversible oxidation of its substrates, and a holdase chaperone activity, by which it maintains its substrates in a folding-competent state before transferring them to either GroEL-GroES or the DnaK-DnaJ-GrpE system for ATP-dependent refolding[16]. We reasoned that identifying the molecular attributes that uniquely allow CnoX to work in concert with GroEL-GroES would lead to new insights into the properties of the GroEL-GroES system.

RESULTS

CnoX and GroEL form a stable complex

To start our investigation, we pulled down CnoX from *E. coli* cellular extracts using specific α-CnoX antibodies. We found that CnoX co-eluted with only one partner (Figure 1A), a ~60-kDa protein identified as GroEL by mass spectrometry (MS), confirming previous results suggesting a direct interaction between the two proteins.[18] In this experiment, CnoX and GroEL were expressed from their native locus in cells grown under normal conditions. Noteworthy, intracellular protein abundance estimates[19] indicate that CnoX and GroEL tetradecamers ($GroEL_{14}$) are expressed at similar levels in rich defined medium at 37°C; thus, there seems to be enough CnoX to satisfy GroEL at a 1:1 CnoX:$GroEL_{14}$ ratio. Exposing the cells to heat shock (42°C) did not lead to an increase in the amount of GroEL that co-eluted with CnoX (Figure S1C).

We then examined whether the CnoX-GroEL interaction could be reconstituted *in vitro* using purified proteins. *E. coli* CnoX and GroEL were independently overexpressed and purified to near homogeneity (Figure S1D). We mixed GroEL and CnoX in a 1:1 molar ratio (1[GroEL subunit]:1[CnoX]) and found that they co-eluted from both a streptavidin affinity column (Figure 1B; a Strep-tag was fused to the N-terminus of CnoX) and a size-exclusion chromatography column (Figure 1C). The latter showed the co-eluting GroEL-CnoX complex in an approximately 14:1 molar ratio compared with the 1:1 input ratio, corresponding to a ratio of 1 CnoX per GroEL double ring. Notably, we also observed that CnoX formed a complex with a GroEL mutant ($GroEL_{R452A/E461A/S463A/V464A}$) known to form a single heptameric ring ($GroEL_7$; Figure S1E).[20] Finally, we determined the affinity between the two proteins using fluorescence spectroscopy and fluorescence anisotropy and found that fluorescein (fluorescein-5-maleimide [FM])-labeled CnoX (FM-CnoX) binds GroEL with a dissociation constant (K_d) of 310 ± 10 nM (Figures 1D and S1F). Using atomic force microscopy (AFM), we measured a specific binding force of 175 ± 75 pN between the two proteins (Figures S1G and S1H). Thus, we conclude that CnoX physically interacts with GroEL and that the two proteins form a stable complex both *in vitro* and *in vivo*.

GroES binding triggers the release of CnoX from GroEL

We next aimed to unravel the interrelationship among CnoX, GroEL, and GroES. GroES reversibly binds GroEL in the presence of nucleotides.[7,11] The addition of adenosine diphosphate (ADP), which triggers conformational changes in GroEL and primes the ring

for GroES binding, had no impact on the GroEL-CnoX complex (purified proteins were mixed in a 14:1 molar ratio) (Figure 1E), although the affinity of CnoX for GroEL decreased slightly (K_d of ~350 nM) (Figure S2A). Strikingly, however, the subsequent addition of GroES (14[GroEL]:14[GroES]:1[CnoX] molar ratio) triggered the release of CnoX from GroEL (Figure 1E), indicating a direct or allosteric competition between CnoX and GroES for GroEL binding. We obtained similar results with a non-hydrolysable ATP analogue (Figure S2B). Next, titration of a complex between GroEL and FM-CnoX with increasing amounts of GroES resulted in a dose-dependent loss of FM-CnoX, confirming that GroES dissociates CnoX from GroEL (Figure S2C). Using a single-site competitive binding model, we calculated a fitted inhibitory constant (K_i) of 47 nM. Finally, under conditions in which GroES was overexpressed, the $GroEL_{R452A/E461A/S463A/V464A}$ variant ($GroEL_7$) did not co-elute with CnoX in pull-down experiments (Figure S2D). Here, we employed $GroEL_7$ for unambiguous data interpretation. Altogether, these results clearly distinguish CnoX from typical GroEL substrates and indicate that CnoX is a *bona fide* GroEL partner. Indeed, GroEL does not release substrate proteins such as unfolded citrate synthase (CS) upon GroES addition (Figure 1E); rather, these proteins become encapsulated inside the GroEL-GroES folding chamber for refolding.[6,7] Along the same line, we found that the presence of CnoX does not prevent GroEL from recruiting unfolded CS (Figure S2E). Thus, CnoX does not restrict access to the substrate-binding site of GroEL.

The C-terminal α-helix of CnoX binds GroEL near the site of substrate entry into the cage

Intrigued by these results, we sought to obtain structural information on the CnoX-GroEL interaction using cryo-electron microscopy (cryoEM). We reconstituted the CnoX-GroEL complex by mixing purified GroEL and $CnoX_{N\text{-}Strep}$ (10[GroEL]:1[CnoX] molar ratio, which corresponds to a ratio of $1[GroEL_{14}]$:1.4 [CnoX]) in the absence of nucleotides. The complex was then affinity-purified (Figure S3A) and imaged for single-particle cryoEM analysis (Figures S3B and S3C and Table S1). Analysis of the two-dimensional (2D) class averages showed the two rings of GroEL stacked back-to-back and revealed the presence of a protruding density on top of the two GroEL rings (Figures 2A, 2B, and S3D). A c7-symmetrical 3D reconstruction resulted in a 3.4 Å electron potential map (Figure S3E) with a density on the GroEL apical domain corresponding to at least five α-helices and allowing an unambiguous rigid body docking with the TPR domain of CnoX (Figures 2C, 2D, S3F, and S3G). The absence of a clearly resolved thioredoxin domain in the CnoX-GroEL complex is consistent with the prior observation of extensive mobility of this domain in the X-ray crystal structure of CnoX alone.[18] This finding suggests that the thioredoxin domain is highly dynamic, which may be relevant for our proposed model (see below).

Although the N-terminal thioredoxin domain of CnoX is not visible, the structure provides crucial molecular details regarding the CnoX-GroEL interaction. First, the structure reveals that CnoX binds GroEL via its C-terminal α-helix (Figure 3A, 3B, 3C); accordingly, a CnoX mutant lacking the last 10 C-terminal residues ($CnoX_{\Delta Cter}$) is unable to bind GroEL, both *in vivo* (Figure 3D) and *in vitro* (Figure S4A). Furthermore, addition of a His-tag to the C-terminus of CnoX ($CnoX_{C\text{-}His}$) or mutation of conserved residues in the C-terminal α-helix ($CnoX_{R277L}$, $CnoX_{Y284L}$) prevented CnoX binding to GroEL (Figures 3D and S4A). Using AFM, we found that the C-terminal α-helix on its own binds to GroEL; we measured

a specific binding force of 135 ± 53 pN between GroEL and the 10 C-terminal residues of CnoX (Figure S1I), which is similar to the binding force measured between full-length CnoX and the chaperonin. We previously reported that CnoX is able to transfer unfolded CS to GroEL-GroES for refolding.[16] As shown in Figure S4B, we found that deleting the last 10 residues of CnoX significantly decreases its ability to cooperate with GroEL for CS refolding. Thus, the C-terminal α-helix of the TPR domain of CnoX functions as a specific GroEL affinity tag that is required and sufficient for GroEL binding and is important for function.

Using cells lacking trigger factor (Δ*tig*) and a functional DnaK-DnaJ-GrpE system (Δ*dnaKdnaJ*), we obtained further *in vivo* evidence that the C-terminal α-helix controls the CnoX-GroEL interaction. Δ*tig*Δ*dnaKdnaJ* cells exhibit a heat-sensitive phenotype that is rescued by overexpression of GroEL-GroES[21], presumably because the chaperonin, when present at high levels, folds proteins that normally depend on trigger factor and/or DnaK-DnaJ-GrpE. We found that overexpressing CnoX, but not $CnoX_{\Delta Cter}$, together with GroEL-GroES prevents the chaperonin from suppressing the growth defect of Δ*tig*Δ*dnaKdnaJ* cells at 37°C (Figure S4C). This result suggests that CnoX, when bound to GroEL, limits the ability of the chaperonin to fold non-substrate proteins. This finding further demonstrates the importance of the C-terminal α-helix and provides additional evidence that the GroEL-CnoX interaction occurs *in vivo*. Finally, we noted that while the sequence of the TPR domain of CnoX is diverse among species, the last C-terminal helix is highly conserved (Figure S4D) and is structurally and electrostatically distinct from the remainder of the TPR domain[18], suggesting that the ability to bind GroEL is widespread and central to CnoX activity.

The structure also reveals where CnoX binds to GroEL; the interaction zone, which has a buried surface area of 472 $Å^2$ (−4.6 kcal/mol; PDBePISA[22]) and encompasses residues D224, K286–M307, K311, D316, R345, and Q348 (Figures 3B and 3C), corresponds to a shallow surface cleft formed by helices J and K in the apical domain of GroEL. This region does not overlap with the substrate-binding site of GroEL in helices H and I[6,7], as also corroborated by the above results (Figure S2E). At least five potential hydrogen bonds or electrostatic interactions stabilize the contacts between CnoX and GroEL (R255-E304, R277-G298, R277-T299, Y284-E304, and Y284-R345, listed as CnoX-GroEL), as well as a hydrophobic interaction between CnoX residues L279, Y280, and L283 and GroEL residues V300, I305, and M307 (Figures 3B and 3C). Accordingly, introducing a set of mutations in the interaction interface of GroEL ($GroEL^{§}$) with CnoX disrupted the GroEL-CnoX interaction (Figure 3E), without affecting the chaperone function of GroEL as the mutant was still able to rescue the temperature sensitivity of Δ*tig*Δ*dnaKdnaJ* cells (Figure S4C).

GroEL is a highly dynamic protein that undergoes substantial conformational rearrangements depending on the binding of a nucleotide, its position in the folding pathway, or the binding of GroES[23]. Comparison of our structure with the different conformational states of GroEL shows that the GroEL rings are in a conformation corresponding to that of the nucleotide-free protein (Figure S4E), as expected. Our findings also indicate that the CnoX-binding paratope remains fully accessible in all conformations, except when GroES is bound (Figure S4E). The persistence of the CnoX-binding site in various

conformations of GroEL is consistent with the ability of CnoX to bind to GroEL irrespective of the presence of a nucleotide (Figures 1B, 1C, 1E, and S2B). Available structures also show a large conformational rotation of the GroEL apical domain in the GroEL-GroES complex. Although the GroES-binding site does not directly overlap with that of CnoX, the conformation of the apical domain results in a steric occlusion of the CnoX-binding paratope (Figure S4E), providing a molecular explanation to our finding that GroES docking onto GroEL is incompatible with CnoX binding (Figures 1E and S2B).

CnoX forms mixed disulfides with obligate GroEL substrates when bound to GroEL

We next aimed to gain insight into the physiological relevance of the CnoX-GroEL complex *in vivo*. GroEL-GroES substrates often need minutes to fold after leaving the ribosome[24], which raises a question regarding how their amino acids are protected from oxidative damage before reaching their native state. This question is particularly relevant for cysteine residues, which are highly sensitive to oxidation by the molecular oxidants present in cells even in the absence of stress.[25,26] Indeed, the thiol side chain of a cysteine is readily oxidized to a sulfenic acid (-SOH), an unstable derivative that can react with another cysteine in the vicinity to form a disulfide or that can be irreversibly oxidized to sulfinic and sulfonic acids. Similar to Anfinsen's experiments showing that noncanonical disulfide pairing thwarts *in vitro* protein folding, one can expect the GroEL chaperonin to require its substrates' cysteines to be reduced for proper folding. CnoX stands out in the proteostasis network in that it combines a chaperone and a redox-protective function;[16] therefore, CnoX may bind GroEL to function as a redox rescue mechanism for slow-folding GroEL-GroES substrates.

By performing additional pull-down experiments, we obtained a crucial result shedding light onto the function of CnoX. When GroEL is pulled down from cellular extracts, it co-elutes with CnoX, as expected. Intriguingly, we found that high-molecular-weight complexes involving CnoX are also pulled down (Figure 4A). When a reducing agent was added, these complexes disappeared, indicating that they correspond to mixed disulfides comprising CnoX and unknown proteins. Accordingly, we did not detect high-molecular-weight complexes when the experiment was repeated with a CnoX mutant lacking the two cysteine residues ($CnoX_{no\_cys}$; Figure 4A), confirming that tripartite complexes of GroEL, CnoX, and unidentified proteins exist in the cell. We identified the proteins involved in the mixed disulfides using MS (Table S2); remarkably, the identified proteins exhibited strong enrichment in GroEL obligate substrates (9 of the 57 obligate GroEL substrates were detected[27]), including two low-abundance proteins, acetylornithine deacetylase, and nicotinamide adenine dinucleotide phosphate (NADP)-specific glutamate dehydrogenase (<400 copies per cell;[19]) (Figure 4B and Table S2). We did not detect these proteins when the experiment was performed using lysates prepared from cells expressing $CnoX_{no\ cys}$. Thus, we conclude that CnoX forms mixed disulfides with obligate GroEL substrates when bound to GroEL in the cell.

CnoX functions as a molecular plugin providing redox quality-control for GroEL substrates

Altogether, our results suggest the following model (Figure 4C). Regardless of stress, CnoX binds GroEL via its highly conserved C-terminal α-helix in a nucleotide-independent

manner. The CnoX-binding interface on GroEL does not overlap with the substrate-binding site. If the substrate that reaches GroEL for folding presents oxidized cysteine residues (to a sulfenic acid or in a disulfide bond), CnoX reacts with the substrate via the cysteines of its thioredoxin domain, resulting in the formation of a mixed disulfide. Cytoplasmic reducing pathways then reduce the mixed disulfide, releasing the substrate in a reduced, folding-competent state. The binding of GroES to GroEL induces conformational changes in the chaperonin and occludes the CnoX-binding site, triggering CnoX release from GroEL and encapsulation of the substrate within the folding cage for folding.

This model implies that segments of unfolded substrates are already present in the cavity of GroEL when the substrates form a mixed disulfide with GroEL-bound CnoX. We confirmed this implication by purifying a tripartite complex of $CnoX_{N\text{-}Strep}$, CS, and GroEL (Figure 5A) and subjecting it to crosslinking MS analysis: we detected crosslinked peptides between several GroEL residues, including four facing the inside of the cavity, and CS (Figures 5B and 5C). Thus, we propose that CnoX functions as a molecular plugin that provides redox quality control for GroEL substrates. Our model is compatible with both the binding of CnoX to unfolded oxidized client proteins in solution followed by delivery to the GroEL chaperonin and the surveillance performed by CnoX to identify erroneously oxidized client proteins that may become stuck at the substrate entrance to the Anfinsen cage of GroEL. This function of CnoX as a quality control plugin for GroEL is constitutive and not inducible by stress. It is not incompatible with the previously reported role of CnoX in the protection of cellular proteins, including GroEL substrates, from HOCl-induced aggregation and oxidation.[16]

DISCUSSION

Investigations of Hsp60 chaperonins started in the 1970s[6], when researchers described mutations that blocked phage head assembly in *groE* and discovered the tetradecameric structure of GroEL, the archetypical member of the Hsp60 family, using EM. Since then, a large body of studies has examined the mechanistic and structural properties of Hsp60 proteins and their Hsp10 co-chaperones, not only in bacteria but also in chloroplasts and mitochondria.[6] This impressive amount of work has rendered chaperonins a textbook example of folding systems. In the current study, the identification of CnoX as a quality-control protein that physically interacts with GroEL-GroES for optimal folding has further widened this field of investigation by uncovering an unsuspected feature of Hsp60. Additional questions remain unsolved and will be the subject of future research. For instance, the biologically active stoichiometry of the CnoX-GroEL complex warrants careful investigation, as well as the specific role of the cytoplasmic reducing pathways in the reduction and release of mixed disulfides. Future work must also establish the location of the N-terminal thioredoxin domain when CnoX is bound to GroEL. Our results show that CnoX forms mixed disulfides with GroEL substrates while being bound to GroEL, but future research will elucidate whether CnoX also functions as a tugboat to locate endangered GroEL substrates in the cytoplasm and escort them to the chaperonin. Finally, it will be important to determine whether similar proteins with a redox quality-control function exist in other organisms, including eukaryotes. The facts that *E. coli* CnoX stably interacts with human mitochondrial Hsp60 (mHsp60; Figure S5A) and that proteins sharing structural

features with CnoX exist in eukaryotes (Figures S5B, S5C, and S5D) support this idea. Along the same line, it is tempting to speculate that living cells could also contain Hsp60 molecular “plugins” with specific, redox-independent functions yet to be discovered.

Limitations of the study

Our study focused on the interaction between CnoX and GroEL. We did not study the ability of CnoX to cooperate with the DnaK-DnaJ-GrpE system. Moreover, although we identified several eukaryotic proteins with structural features similar to those of CnoX —which suggest that these proteins could function as molecular plugins for eukaryotic Hsp60 proteins— we did not investigate this attractive hypothesis. Our model implies that cytoplasmic reducing systems catalyze the reduction of mixed disulfides between CnoX and its substrates. The respective roles of the thioredoxin and glutaredoxin pathways in this process remain to be determined. Further studies are also required to obtain additional structural information on the ternary complexes between GroEL, CnoX, and their substrates.

STAR*Methods

RESOURCE AVAILABILITY

Lead contact—Further information and requests for resources and reagents should be directed to and will be fulfilled by the lead contact, Jean-François Collet (jfcollet@uclouvain.be).

Materials availability—Strains and plasmids generated in this study are available upon request to the lead contact.

Data and code availability

- Coordinates and electron potential maps for the GroEL:CnoX cryoEM structure have been deposited in the PDB and EMDB under accession codes 7YWY and EMD-14352, respectively.
- Raw data from Figures 1, 2, 3, 4, 5 and Supplemental Figures 1, 2, 3, 4, 5, 6 were deposited on Mendeley at http://dx.doi.org/10.17632/9pt4v7hc93.1.
- Any additional information required to reanalyze the data reported in this paper is available from the lead contact upon request.

EXPERIMENTAL MODEL AND SUBJECT DETAILS

The *E. coli* strains used in this study are listed in Table S3. We prepared the *cnoX* deletion mutant by transferring the corresponding allele (*ybbN*::kan^{R}) from the Keio collection [29] into MG1655 by P1 phage transduction, with verification by polymerase chain reaction (PCR). To excise the kanamycin-resistance cassette, we used pCP20 [30]. Unless otherwise indicated, we grew the cells in lysogeny broth (LB) at 37°C, and when necessary, we supplemented the growth media with ampicillin (100–200 μg/mL), chloramphenicol (100 μg/mL), or kanamycin (50 μg/mL).

METHOD DETAILS

Plasmid construction—Table S4 shows the plasmids used in this study. The primers used for their construction are shown in Table S5. To obtain high expression levels of wild-type CnoX, $CnoX_{C\text{-}His}$, GroEL, and GroES, we cloned the corresponding genes into the high copy vector pET22b(+) (Novagen). DNA encoding $CnoX_{N\text{-}Strep}$ was cloned into the medium copy vector pACYCDuet-1. To prepare an expression vector for *cnoX* without the last 10 C-terminal residues ($CnoX_{\Delta Cter}$), we amplified the corresponding sequence from *E. coli* genomic DNA and ligated the sequence into pET22b(+). The CnoX and GroEL substitution variants used in this study were generated by site-directed mutagenesis, except for $GroEL_{G298A/T299L/V300K/E304L/I305K/M307K/R345L}$, which was generated using Gibson assembly. We generated the $CnoX_{N\text{-}link/C38A/C63A}$ variant using site-directed mutagenesis by inserting the coding sequences of Met, Ala, Cys, Ala, and Gly residues at the N-terminal extremity. To prepare an expression vector for mHsp60, we amplified the corresponding sequence from the MAC_C_CH60 vector (Addgene) without the mitochondrial targeting sequence, which was replaced by the coding sequences of Met, Gly, and Ser residues, and cloned the sequence into pET22b(+) using Gibson assembly.

Expression and purification of CnoX, $CnoX_{\Delta Cter}$, $CnoX_{N\text{-}Strep}$, $CnoX_{C\text{-}His}$, and $CnoX_{N\text{-}link/C38A/C63A}$

We utilized *E. coli* BL21 (DE3) carrying pET22b_cnoX, pET22b_$cnoX_{\Delta Cter}$, or pET22b_$cnoX_{N\text{-}link/C38A/C63A}$ to overexpress wild-type CnoX, $CnoX_{\Delta cter}$, or $CnoX_{N\text{-}link/C38A/C63A}$, respectively. Cells grew at 37°C until the optical density at 600 nm (OD_{600}) reached 0.5, and then, we added 1 mM IPTG for 3 h to induce protein expression. Cells were pelleted, resuspended in 50 mM Tris-HCl pH 8, and disrupted with a French press. After centrifugation for 30 min at 40,000*g* at 4°C, the supernatant was filtered through 0.45-μm filters and loaded onto a 5-mL Q-Sepharose HP column (GE Healthcare). We eluted the proteins with a 0%–50% gradient of 1 M NaCl in 50 mM Tris-HCl pH 8. Proteins underwent a second purification step via a HiLoad 16/60 Superdex 75 gel filtration system (GE Healthcare) and were eluted in 10 mM hydroxyethyl piperazineethanesulfonic (HEPES)-KOH pH 8, 100 mM NaCl.

We employed *E. coli* BL21 (DE3) carrying pET22b-$cnoX_{C\text{-}His}$ to overexpress CnoX fused to a C-terminal His-tag ($CnoX_{C\text{-}His}$). Cells grew at 37°C until an OD_{600} of 0.5 was reached, and we added 1 mM IPTG for 3 h to induce protein expression. Cells were pelleted, resuspended in buffer A (NaPi 50 mM pH 8, 300 mM NaCl), and lysed with a French press. After centrifugation for 30 min at 40,000*g* at 4°C, the supernatant was filtered through 0.45-μm filters and loaded on Ni-nitriloacetic acid (NTA) agarose beads (5 mL; IBA Lifesciences) previously equilibrated with buffer A. After washing the resin with buffer A supplemented with 20 mM imidazole, we eluted the proteins with buffer A supplemented with 300 mM imidazole. As a final purification step, we performed size-exclusion chromatography using a HiLoad 16/60 Superdex 75 column (GE Healthcare) with 10 mM HEPES pH 7, 100 mM NaCl.

E. coli BL21 (DE3) cells carrying pACYCDuet-1-$cnoX_{N\text{-}Strep}$ were used to express CnoX fused to an N-terminal Strep-tag ($CnoX_{N\text{-}Strep}$). Cells grew at 37°C until an OD_{600} of

0.5 was reached, and we added 1 mM IPTG for 3 h to induce protein expression. Cells were pelleted, resuspended in buffer B (50 mM Tris-HCl pH 8, 150 mM NaCl), and lysed with a French press. After centrifugation for 30 min at 40,000*g* at 4°C, the supernatant was filtered through 0.45-μm filters and loaded onto a 5-mL Strep-Tactin column (IBA Lifesciences) previously equilibrated in buffer B. After applying a washing step with buffer B, we performed elution with buffer B supplemented with 2.5 mM D-desthiobiotin. We then purified the sample using size-exclusion chromatography on a HiLoad 10/300 Superdex 200 column (GE Healthcare) using buffer B supplemented with 1 mM ethylenediaminetetraacetic acid (EDTA).

Expression and purification of GroEL, GroEL variants, and GroES

We used *E. coli* BL21 (DE3) cells carrying pET22b-groL to overexpress GroEL. Cells grew at 37°C until an OD_{600} of 0.5 was reached, and we added 1 mM IPTG for 3 h to induce protein expression. Cells were pelleted, resuspended in buffer C containing 50 mM Tris-HCl pH 7.4, 1 mM EDTA, and 1 mM DTT, and lysed with a French press. After centrifugation for 30 min at 40,000*g* at 4°C, the supernatant was filtered through 0.45-μm filters, loaded onto a 5-mL DEAE-Sepharose HP column (GE Healthcare), and eluted in a gradient (0%–50%) of 1 M NaCl in buffer C. The second purification step required gel filtration using a HiLoad S200 16/600 column (GE Healthcare) and elution buffer containing 10 mM HEPES-KOH pH 8, 100 mM NaCl, and 1 mM DTT. Finally, we loaded the protein onto a 5-mL Q-Sepharose HP column (GE Healthcare) using a gradient (0%–50%) of 1 M NaCl in buffer C. $GroEL_{D490C}$, $GroEL_{R452A/E461A/S463A/V464A}$, and $GroEL_{G298A/T299L/V300K/E304L/I305K/M307K/R345L}$ ($GroEL^{\S}$) Were purified in a similar manner.

We utilized *E. coli* BL21 (DE3) carrying pET22b-groS to overexpress GroES. Cells were grown at 37°C. When an OD_{600} of 0.5 was reached, we added 1 mM IPTG for 3 h to induce protein expression. Cells were pelleted, resuspended in buffer D (30 mM Tris-HCl pH 7.5, 10 mM NaCl, 1 mM EDTA), and lysed with a French press. After centrifugation for 30 min at 40,000*g* at 4°C, the supernatant was filtered (0.45-μm filters), loaded onto a 5-mL DEAE-Sepharose HP column (GE Healthcare), and eluted in a 0%–50% gradient of 1 M NaCl in buffer D. For the second purification step, we loaded the sample onto a 5-mL Q-Sepharose HP column (GE Healthcare) and eluted the proteins with a 0%–50% gradient of 1 M NaCl in 20 mM imidazole pH 5.8. Finally, we loaded the sample onto a gel filtration column (HiLoad S200 26/60 column [GE Healthcare]) equilibrated in buffer D.

For all proteins, we verified the purity via SDS-PAGE with Coomassie staining and concentrated samples using a Vivaspin Turbo (Sartorius) with a 5-kDa molecular-weight cutoff. We assessed protein concentrations by measuring the absorbance at 280 nm using a Varian Cary 50 UV-Vis spectrophotometer.

Reconstitution of the GroEL-$CnoX_{N\text{-}Strep}$ complex

To reconstitute GroEL-$CnoX_{N\text{-}Strep}$, we mixed GroEL (150 μM) in excess (10:1) or with equimolar amounts of $CnoX_{N\text{-}strep}$ in 500 μL of buffer A. After 15 min at room temperature, the mixture was loaded onto a 1-mL Strep-Tactin column (IBA Lifesciences) previously

equilibrated in buffer A. After applying a washing step with buffer A, we performed elution with buffer A supplemented with 2.5 mM D-desthiobiotin.

Expression and purification of the GroEL-CS-CnoX$_{N\text{-}strep}$ complex

We used *E. coli* BL21 (DE3) cells carrying pACYCDuet-1-cnoX$_{N\text{-}strep}$_gltA_groL to overexpress CnoX$_{N\text{-}Strep}$, CS, and GroEL. Cells were grown at 37°C. When an OD_{600} of 0.5 was reached, we added 1 mM IPTG for 4 h to induce protein expression. Cells were pelleted, resuspended in buffer B (50 mM Tris-HCl pH 8, 150 mM NaCl) supplemented with 1 mM EDTA, and lysed with a French press. After centrifugation for 20 min at 17,418*g* at 4°C, the supernatant was filtered through 0.45-μm filters and loaded onto a 2-mL Strep-Tactin column (IBA Lifesciences) previously equilibrated in buffer B. After applying a washing step with buffer B, we performed elution with buffer B supplemented with 2.5 mM D-desthiobiotin. We then purified the sample using size-exclusion chromatography on a HiLoad 10/300 Superdex 200 column (GE Healthcare) using buffer B supplemented with 1 mM EDTA.

In vivo pull-down of CnoX

E. coli MG1655 wild-type, *E. coli* MG1655 Δ*cnoX*, and *E. coli* MG1655 cells carrying pET22b-cnoX, pET22b-cnoX$_{\Delta Cter}$, pET22b-cnoX$_{R277L}$, pET22b-cnoX$_{Y284L}$, or pET22b-cnoX$_{C\text{-}His}$ grew in LB (25 mL) at 37°C in a shaking incubator until the mid-log phase was reached. The cells were then harvested, resuspended in 1 mL of buffer E (50 mM Tris-HCl pH 7.4, 150 mM NaCl, 1 mM EDTA), and sonicated. After a 5-min centrifugation at 16,000*g* at 4°C, we added 5 μL of undiluted rabbit anti-CnoX antibody and 50 μL of protein A/G magnetic beads (Pierce) to the supernatant to immunoprecipitate CnoX; then, we incubated the samples for 30 min on a wheel at room temperature. After three washes with 500 μL of buffer E, CnoX was eluted with 20 μL of 100 mM glycine pH 2.5. We neutralized the samples with 2 μL of 1.5 M Tris-HCl pH 8 before SDS-PAGE analysis and Coomassie staining.

In vitro pull-down of GroEL

We mixed GroEL (5 μM) with equimolar amounts of either CnoX, CnoX$_{\Delta Cter}$, CnoX$_{C\text{-}His}$, or CnoX and unfolded CS in 100 μL of buffer E. After 30 min at room temperature, we immunoprecipitated GroEL by adding 5 μL of undiluted rabbit anti-GroEL antibody and 50 μL of protein A/G magnetic beads (Pierce); samples were incubated for 30 min on a wheel at room temperature. After three washes with buffer E, GroEL was eluted with 20 μL of 100 mM glycine pH 2.5. We then neutralized the samples with 2 μL of 1.5 M Tris-HCl pH 8 before SDS-PAGE analysis and Coomassie staining.

In vitro pull-down of CnoX

CnoX, CnoX$_{\Delta Cter}$, or CnoX$_{C\text{-}His}$ (5 μM) was mixed with equimolar amounts of GroEL in 100 μL of buffer E. After 30 min at room temperature, we immunoprecipitated CnoX by adding 5 μL of undiluted rabbit anti-CnoX antibody and 50 μL of protein A/G magnetic beads (Pierce); then, we incubated the samples for 30 min on a wheel at room temperature. After three washes with buffer E, CnoX was eluted with 20 μL of 100 mM glycine pH 2.5.

We neutralized the samples with 2 μL of 1.5 M Tris-HCl pH 8 before SDS-PAGE analysis and Coomassie staining.

Size-exclusion chromatography analysis

To reconstitute GroEL-CnoX, we mixed both proteins using the ratios indicated in the manuscript. After 15 min at room temperature, the sample was loaded onto a Superdex S200 10/300 column equilibrated with buffer E. The fractions corresponding to absorbance peaks at 280 nm were collected and analyzed by gradient (4%–12%) SDS-PAGE.

To determine the impact of GroES addition on the GroEL-CnoX complex, we mixed GroEL (45 μM) with CnoX using the ratios indicated in the manuscript in 1 mL of buffer F (50 mM Tris-HCl pH 8, 150 mM KCl, 10 mM $MgCl_2$, 1 mM DTT, 1 mM EDTA) supplemented with either ADP (1 mM) or AMP-PNP (1 mM). After 15 min at room temperature, GroES was added at a molar ratio of 14:1:14 (GroEL:CnoX:GroES). After 15 min, we loaded the sample onto a Superdex S200 10/300 column equilibrated with buffer A supplemented with ADP (50 μM) or AMP-PNP (50 μM). The column ran at a flow rate of 0.5 mL/min with 1-mL fractions using an AKTA Purifier (Cytiva). Fractions corresponding to absorbance peaks at 280 nm were collected and analyzed by gradient (4%–12%) SDS-PAGE.

To investigate the binding of CS on GroEL, CS (82 μM, Sigma-Aldrich) was unfolded by dilution in 4 M guanidinium chloride and incubated at room temperature for 2 h. To assay binding on GroEL, we mixed GroEL (45 μM) with unfolded CS (CS_{denat}) at a molar ratio of 14:1 GroEL:CS_{denat} in 1 mL of buffer F supplemented with 1 mM ADP. After 15 min at room temperature, GroES was added at a molar ratio of 14:1:14 GroEL:CS_{denat}:GroES; after another 15 min, we loaded the mixture onto a Superdex S200 10/300 column equilibrated with buffer A supplemented with 50 μM ADP. The column ran at a flow rate of 0.5 mL/min with an AKTA Purifier, and 1-mL fractions were collected. The fractions corresponding to absorbance peaks at 280 nm were collected and analyzed by gradient (4%–12%) SDS-PAGE.

Purification of GroEL, GroES, and CnoX for quantitative binding studies

CnoX and GroES were expressed and purified as previously described [18]. Purified proteins had their N-terminal hexahistidine tags removed by thrombin cleavage and were passed again over Ni^{2+}-NTA resin. These proteins were then collected in the flow-through, dialyzed into storage buffer (25 mM HEPES pH 7.5, 100 mM KCl), snap-frozen in 50- to 100-μL aliquots in liquid nitrogen, and stored at −80°C. We verified tag removal by electrospray MS. We induced GroEL expression from pET15b as an untagged protein by removing the sequence between the “CC” of the NcoI site and the “ATG” of the NdeI site using mutagenic PCR primers (see Table S5). GroEL lacking any tag- or vector-derived amino acids was expressed by 0.5 mM IPTG induction, and cells were harvested by centrifugation as described. After sonication and centrifugation at 12000*g*, clarified lysate was loaded onto a Macro-Prep High Q resin (Bio-Rad) column, and proteins were eluted over a 0.1–1.1 M NaCl gradient in 25 mM HEPES pH 7.5. The fractions ran on SDS-PAGE gels, and those enriched in GroEL were pooled. We precipitated the crude GroEL fraction by gradually adding finely ground $(NH_4)_2SO_4$ powder to 75% saturation at room temperature

and centrifuging the fraction at 20,000*g* for 45 min. The pellet was then dissolved in storage buffer (25 mM HEPES pH 7.5, 100 mM KCl) and dialyzed against storage buffer overnight. GroEL was applied to a Sephacryl S-300 HR gel filtration column and eluted near the void volume due to the large size of the GroEL oligomer. We identified the fractions containing GroEL by SDS-PAGE and then pooled and dialyzed the fractions against 50 mM Tris-HCl pH 7.5, 1 mM EDTA, 30% methanol (Tris-methanol buffer). The pooled GroEL fractions were loaded onto a UNO Q12 anion exchange column (Bio-Rad) and eluted with a gradient of 0–1 M NaCl in Tris-methanol buffer. We identified GroEL-containing fractions by SDS-PAGE, and those lacking any visible contaminants were pooled, dialyzed into storage buffer, concentrated by centrifugation with a 10-kDa molecular-weight cutoff concentrator, snap-frozen in 50- to 100-μL aliquots in liquid nitrogen, and stored at −80°C.

Fluorescent labeling of CnoX

We fluorescently labeled CnoX using FM (Thermo Fisher Scientific) for binding studies. The maleimide moiety of FM is cysteine-reactive and is therefore expected to label the N-terminal thioredoxin-like domain of CnoX, which contains the only two cysteine residues in the protein, Cys38 and Cys63. A 25-fold molar excess of FM to CnoX in 20 mM sodium phosphate buffer pH 7.2, 150 mM NaCl, and 5 mM EDTA was incubated for 4 h at room temperature in the dark. We then dialyzed the sample using 3.5-kDa-cutoff regenerated cellulose tubing against storage buffer overnight at 4°C to remove any unreacted FM.

We determined the stoichiometry of FM-CnoX labeling via the ratio of absorbance at 495 nm and 280 nm.

$$\text{Labeling stoichiometry} = \frac{\frac{A_{495}}{\varepsilon_{495}^{FM}}}{\frac{\left(A_{280} - \left(A_{495}\frac{\varepsilon_{280}^{FM}}{\varepsilon_{495}^{FM}}\right)\right)}{\varepsilon_{280}^{CnoX}}}$$

The calculated ε_{280} for CnoX is 23,000 M^{-1} cm^{-1} (ExPASY), the ε_{495} of FM is 75,000 $M^{-1}cm^{-1}$, and the ratio of FM extinction coefficients at 280 and 495 nm ($\frac{\varepsilon_{280}^{FM}}{\varepsilon_{495}^{FM}}$; sometimes called the correction factor) is 0.3. The labeling stoichiometry is 2.2 FM per CnoX molecule, as expected for the two cysteine residues in the N-terminal thioredoxin domain. FM-CnoX was snap-frozen in liquid nitrogen and stored at −80°C.

Measurement of the CnoX-GroEL binding affinity

We performed fluorescence measurements on a Cary Eclipse fluorescence spectrophotometer (Varian) at room temperature (~22°C). We measured fluorescence emission spectra between 500 and 560 nm with an excitation wavelength of 495 nm. The excitation and emission slits were set to 5 nm, and spectra were recorded at a scan rate of 10 nm/s. To measure the binding of GroEL to FM-CnoX, we titrated 119 μM GroEL into 0.5 μM FM-CnoX in a total volume of 0.5 mL storage buffer. Final GroEL concentrations ranged from 0.035 to 1 μM. We calculated the normalized fluorescence ratio (D) as:

$$D = \frac{F_i}{F_0} - 1$$

where F_i is the fluorescence emission of FM-CnoX at peak (typically 520 nm) measured after the addition of GroEL and F_0 is the fluorescence emission at peak measured for FM-CnoX alone.

To complement the fluorescence emission measurements, we performed a fluorescence anisotropy binding assay using a Jasco J-815 CD spectrophotometer at 20°C. We employed an excitation wavelength of 495 nm and a 540-nm emission filter. Measurements were collected using a cell with a 1-cm path length at a scan rate of 0.833 nm/s from 450 to 550 nm. In a total volume of 2 mL of storage buffer, we titrated 0.5 μM FM-CnoX with 119 μM GroEL to final concentrations ranging from 0.036 to 1 μM. The final volume change after GroEL titration was less than 1%. We measured the fluorescence anisotropy for each titration point 2 min after the addition of GroEL. The data were averaged from 3–4 measurements. Binding data were plotted and fitted in Prism (GraphPad) using nonlinear least-squares minimization. We utilized a single-site binding model with positive cooperativity for the CnoX-GroEL interactions and a single-site competition model with a logarithmic competitor concentration for the GroES competition experiment. No data linearization was performed.

Influence of nucleotides on the CnoX-GroEL and GroES interaction

To examine the effect of ATP or ADP on GroEL-CnoX binding, we repeated the experiment described in the previous section using 0.5 μM FM-CnoX and GroEL in storage buffer with 2 mM ATP (Alfa Aesar) or 2 mM ADP (Sigma) and 10 mM $MgCl_2$. For the GroES competition experiment, 0.5 μM FM-CnoX was incubated with 0.5 μM GroEL, with or without 2 mM ATP in storage buffer, and then titrated with GroES to final concentrations ranging from 0.035 to 2 μM. We measured the fluorescence emission at peak 2 min after adding titrated protein at room temperature. In all titrations, the final volume change was less than 1%; hence, no dilution correction was performed. Data were averaged from 3–4 measurements.

In vivo trapping of GroEL-CnoX-substrate tripartite complexes

To identify proteins trapped in a mixed disulfide with CnoX when CnoX is bound to GroEL, we immunoprecipitated GroEL from extracts prepared from *E. coli* BL21 (DE3) cells carrying pET22b-cnoX and pET22b-cnoX$_{C38A/C63A}$ as follows. After an overnight preculture, cells were diluted in 500 mL of LB containing 100 mg/mL ampicillin and grown at 37°C. At the mid-log phase, we induced protein expression for 1 h with 1 mM IPTG. Cultures were cooled on ice for 10 min, and iodoacetamide (25 mM) was added. After 30 min, the cells were harvested, resuspended in 20 mL of buffer E, and sonicated. After performing centrifugation at 12,000*g* at 4°C, we added 150 μL of undiluted rabbit anti-GroEL antibody and 1 mL of protein A/G magnetic beads (Pierce) to the supernatant. After 30 min on a wheel at room temperature, magnetic beads were collected and resuspended

with 1 mL of buffer E. After applying three washes with 1 mL of buffer E, we eluted GroEL with 100 μL of 0.1 M glycine pH 2.5.

Chaperone-mediated reactivation of chemically unfolded CS

We adapted our protocol from Haslbeck and Buchner (2015) and Hoffmann et al. (2004). Briefly, 15 mM CS (Sigma-Aldrich) was unfolded by dilution in 4 M guanidinium chloride in Tris-EDTA buffer (50 mM Tris-HCl [pH 8], 2 mM EDTA) and incubated at 16°C for 2 h. We diluted the unfolded CS by 1:160 (final concentration of 75 nM) in 40 mM HEPES-KOH (pH 8), 10 mM KCl, and 2 mM Mg-ATP (unless otherwise specified) containing 0 or 0.45 mM YbbN. After a 20-min incubation at 25°C, the DnaK/DnaJ/GrpE refolding system (0.4 mM, 0.16 mM, and 0.4 mM, respectively) or the GroEL14/GroES7 refolding system (0.15 mM and 0.5 mM, respectively) was added to the refolding solution and incubated for 2 h at 25°C. We added 4 mL of this mixture to 200 mL of reaction buffer (100 mM oxaloacetic acid, 100 mM 5,5'-dithiobis(2-nitrobenzoic acid), and 160 mM acetylCoA in Tris-EDTA buffer) in a 96-well plate. We monitored the absorbance at 412 nm for 1 min with a Biotek Synergy H1 Hybrid microplate reader and used the initial slope of the absorbance values to calculate the CS activity.

Bacterial viability assay

E. coli MC4100 Δ*tig*Δ*dnaKdnaJ* cells carrying p29SEN-EV, p29SEN-groSgroL, p29SEN-groSgroL$_{heptuple}$, p29SEN-groSgroLcnoX, or p29SEN-groSgroLcnoX$_{\Delta Cter}$ grew in LB supplemented with ampicillin at 20°C until the mid-log phase was reached. Cells were serially diluted and spotted on LB agar plates containing ampicillin, with or without 100 μM IPTG, overnight at 37°C.

AFM

Gold-coated glass coverslips and cantilevers (OMCL-TR4, Olympus Ltd.; nominal spring constant of ~0.02 N m^{-1}) were incubated with 0.1 mg mL^{-1} of CnoX$_{N\text{-}link/C38A/C63A}$, the last C-terminal 10 amino acids of CnoX fused to a linker (CGGGSGGGYRRQLYALLY), or GroEL$_{D490C}$ solution for 1 h, rinsed with buffer D, and then immediately used without dewetting. We performed measurements at room temperature in 50 mM Tris pH 8, 150 mM NaCl, 1 mM EDTA with a Force Robot 300 AFM (JPK Instruments). We recorded multiple (32 × 32) force–distance curves over an area of 500 x 500 nm^2 with an applied force of 250 pN, a constant approach, and a retraction speed of 1,000 nm s^{-1}. A histogram was generated based on the force of the last rupture event for each curve. We measured the spring constants of the cantilevers by the thermal noise method and analyzed these data with data-processing software from JPK Instruments.

Native PAGE

We performed Blue native electrophoresis analysis of the concentrated complex on a 3% □ 12% Bis-Tris gel (Life Technologies) following the manufacturer's instructions. We identified the protein complex bands separated in the native electrophoresis via SDS-PAGE. Briefly, bands of interest were excised, boiled in SDS-PAGE sample buffer, and applied to the top of a polyacrylamide gel.

Immunoblotting

Samples were boiled before being loaded onto a precast NuPAGE Bis-Tris 12% gel (Life Technologies). We performed immunoblotting according to standard procedures using 1:5000 anti-CnoX antibody (rabbit serum, CER group, Belgium) followed by a horseradish peroxidase-conjugated anti-rabbit antibody (Sigma). We conducted chemiluminescence imaging (ECL Prime Western Blotting Detection Reagents; GE Healthcare) with an ImageQuant LAS 500 Camera (GE Healthcare Life Sciences).

Mammalian homologs of CnoX

The CnoX structure (http://pfam.xfam.org/protein/P77395) is organized into three domains, corresponding to the Pfam entries *Thioredoxin* (http://pfam.xfam.org/family/Thioredoxin), *TPR_19* (http://pfam.xfam.org/family/TPR_19), and *TPR_20* (http://pfam.xfam.org/family/TPR_20). As of March 9, 2022, these Pfams contain 40,361 (*Thioredoxin*), 10,056 (*TPR_19*), and 44 (*TPR_20*) eukaryotic sequences. We downloaded all 44 eukaryotic sequences from UniProt [31] and built corresponding AlphaFold 3D models using ColabFold [32]. Most of these models contained all three domains (*Thioredoxin*, *TPR_19*, and *TPR_20*). Three representative structures are shown in Figure S5.

Protein identification by MS

After in-gel digestion with trypsin, peptides were dissolved in solvent A (0.1% trifluoroacetic acid in 2% acetonitrile), directly loaded onto a reversed-phase precolumn (Acclaim PepMap 100, Thermo Fisher Scientific), and eluted in backflush mode. We performed peptide separation using a reversed-phase analytical column (Acclaim PepMap RSLC, 0.075 x 250 mm, Thermo Fisher Scientific) with a linear gradient of 4%–27.5% solvent B (0.1% formic acid in 98% acetonitrile) for 40 min, 27.5%–50% solvent B for 20 min, 50%–95% solvent B for 10 min, and holding at 95% for the last 10 min at a constant flow rate of 300 nL/min on an Ultimate 3000 RSLC system. We analyzed the peptides by an Orbitrap Fusion Lumos tribrid MS (Thermo Fisher Scientific). The peptides were subjected to a nanospray ionization source followed by MS/MS in a Fusion Lumos coupled online to a nano-LC. Intact peptides were detected in the Orbitrap at a resolution of 120,000. We selected peptides for MS/MS using a higher-energy collision dissociation setting of 30 and detected ion fragments in the Orbitrap at a resolution of 30,000. A data-dependent procedure that alternated between one MS scan and one MS/MS scan was applied for 3 s for ions above a threshold ion count of 2.0×10^4 in the MS survey scan with 40.0-s dynamic exclusion. An electrospray voltage of 2.1 kV was applied. We obtained MS1 spectra with an automatic gain control target of 4×10^5 ions and a maximum injection time of 50 ms and MS2 spectra with an automatic gain control target of 5×10^4 ions and a maximum injection set to dynamic. For MS scans, the m/z scan range was 375–1800. We processed the resulting MS/MS data using the Sequest HT search engine within Proteome Discoverer 2.4 SP1 against an *E. coli K12* protein database obtained from Uniprot (4,349 entries). Trypsin was specified as a cleavage enzyme allowing up to two missed cleavages, four modifications per peptide, and up to five charges. We set the mass error to 10 ppm for precursor ions and 0.1 Da for fragment ions. Oxidation on Met (+15.995 Da) and conversion of Gln (−17.027 Da) or Glu (−18.011 Da) to pyro-Glu at the peptide N-terminal were considered as variable

modifications. We assessed the false discovery rate using Percolator, with the thresholds for proteins, peptides, and modification sites specified at 1%. For abundance comparison, we calculated abundance ratios by label-free quantification of the precursor intensities within Proteome Discoverer 2.4 SP1.

Crosslinking identification by MS

We applied 100 µL of the purified ternary complex between CS, CnoX, and GroEL onto a NAP-5 column for buffer exchange into 500 µL of 20 mM HEPES pH 8. Then, DSSO was not added or added to the protein sample at a final concentration of 2 mM. After 60 min at room temperature, we ended the reaction by adding 40 mM of Tris pH 8. Protein extraction and digestion with trypsin were performed as in [33]. Briefly, protein samples were precipitated by adding three volumes of methanol, one volume of chloroform, and three volumes of water, vortexed, and centrifuged at 15,000*g* for 2 min at room temperature. The supernatant was removed carefully and the precipitated protein layers at the interface were further washed and pelleted by adding three volumes of methanol and centrifuging at 15,000*g* for 2 min. Subsequently, the protein pellets were air-dried for 10 min after removing the methanol. The protein pellets were then resuspended in 200 µL of a buffer containing 4 M urea, 50 mM NH_4HCO_3 and sonicated at 80 % amplitude (20 kHz) for 30 s. The protein suspension was reduced by 5 mM tris(2-carboxyethyl)-phosphine (TCEP) at 55 °C for 20 min and then alkylated by 10 mM iodoacetamide in the dark at 25 °C for 20 min with vigorous shaking using a Thermomixer Eppendorf Comfort at 1000 rpm. Afterwards, the proteins were digested by adding 250 µL 50 mM NH_4HCO_3, 2.5 µL 1 % ProteaseMAX™ Surfactant dissolved in 50 mM NH_4HCO_3, and 1:100 (enzyme/protein, w/w) Sequencing Grade Modified Trypsin to reach a final reaction volume of 500 µL. The digestion reactions were incubated overnight at 37 °C with vigorous shaking using a Thermomixer Eppendorf Comfort. The next day, the protein digestion reactions were stopped by adding trifluoroacetic acid (TFA) to 0.1 % final concentration. We then conducted size-exclusion enrichment of crosslinked peptides on a Vivaspin membrane with a 5-kDa cutoff (Sartorius). Peptide separation was performed on an Ultimate 3000-nLC RSLC essentially as described in [33] except that the analytical column was a C18 reversed-phase nano-analytical column (BioZen Polar-C18, 250 x 0.075 mm, Phenomenex). We subjected the peptides to a nanospray ionization source followed by tandem MS/MS in a tribrid Fusion Lumos Orbitrap analyzer coupled online to a nano-LC. Spectra were acquired by an XLMS Clevable MS2-MS3 scan routine specific for DSSO Xlinks with MS1 and MS2 detection in the Orbitrap and MS3 in the Ion Trap. In summary, we acquired full MS1 spectra at a resolution of 120,000 and MS2 scans at a resolution of 30,000. The first MS2 scan was performed in data-dependent acquisition mode with collision-induced dissociation (CID) fragmentation and analysis of the daughter ions in the Orbitrap. If a targeted mass difference specific for DSSO (31.9721 Da) was detected in an ion pair, this finding would trigger a supplemental MS2 fragmentation of the same parent ion by EThcD and several MS3 scans for both ions in the pair by CID fragmentation. We processed the resulting MS/MS data using Sequest HT and the Xlink 2.5 search engine within Proteome Discoverer 2.5 against an *E. Coli* protein database obtained from Uniprot (4,353 entries) and a specific homemade library containing six proteins (groEL, cnoX, tufB, ompA, gltA, lpp) for Xlink identification. Trypsin was specified as a cleavage enzyme

allowing up to two missed cleavages, four modifications per peptide, and up to seven charges. We set the mass error to 10 ppm for precursor ions and 0.02 Da for fragment ions. Oxidation on methionine, carbamidomethyl on cysteine, and DSSO monolinks were considered as variable modifications. We assessed the false discovery rate using Percolator and set specified thresholds for proteins, peptides, and modification sites at 1%.

Single-particle cryoEM imaging and data processing

Prior to vitrification, we assessed the sample quality using negative-stain EM. For this step, 3 μL GroEL-CnoX at 0.4 mg/mL was applied to a glow-discharged formvar Cu400 grid (Electron Microscopy Sciences) and screened using in-house 120-kV JEOL JEM 1400 and 1400+ microscopes equipped with an LaB_6 filament at the VIB-VUB BECM facility. We vitrified the GroEL-CnoX sample in liquid ethane using a CP3 Cryoplunge (Gatan) set to 100% humidity and room temperature. R2/1 (Quantifoil) grids were coated with graphene oxide (Sigma), and a 3-μL sample at 0.4 mg/mL was applied and manually back-blotted for 4 s before plunging.

We collected data on an in-house (BECM) 300-kV JEOL CRYOARM 300 equipped with a K3 direct electron detector (Gatan). We collected 3,015 movies in counting mode, with a dose of 68.27 e/Å^2 spread over 61 frames at a nominal magnification of 60.000X, corresponding to a pixel size of 0.784 Å. Images were motion-corrected via MotionCor2.1 [34] using 5 x 5 patches with dose-weighting, and the contrast transfer function was estimated using ctffind4.1 [35]. We picked particles using crYOLO 1.5 [36] with a dataset-specific trained crYOLO network on six micrographs (709 picked particles). The picking quality and CnoX occupancy were assessed using ISAC2 [37] as implemented in the SPHIRE package [38].

We performed all subsequent processing using RELION3.0 [39]. A total of 670,080 picked particles were extracted with a box size of 400 and were binned twice for processing. A c1 initial 3D model was generated *ab initio*. In all subsequent steps, we applied c7 symmetry throughout. After extensive rounds of 3D classification to optimize the density for CnoX on GroEL, we utilized 170,458 particles for the final reconstruction at 3.4 Å.

Final maps were density-modified using phenix.resolve [40], and the model was fitted and symmetry-expanded in UCSF Chimera [41] using the second TPR domain of CnoX (helices 2_A-2_A'-2_B-2_B'-2_C [197-284] from PDB: 3QOU) and GroEL (pdb:1XCK) as starting coordinates. We conducted further docking and refinement using phenix.real.space [42] with manual curation in COOT.[43] After the first refinement, we generated a second local resolution-sharpened map using LocScale [44], as implemented in the CCPEM project package [45]. We used this map together with the density-modified map to aid further map building and refinement in Phenix [46]. The reported FSC-model curve, resolution, and local-resolution maps were calculated using the Phenix validation output and the Phenix implementation of local-resolution assessment.

QUANTIFICATION AND STATISTICAL ANALYSIS

We performed statistical analysis using GraphPad Prism 6. Results are represented as the mean ± standard error of the mean. We conducted comparisons of two groups using

unpaired two-tailed Student's t-tests with an assumed Gaussian distribution and equal variances. Experiments were performed in triplicate (n = 3) unless otherwise indicated.

Supplementary Material

Refer to Web version on PubMed Central for supplementary material.

ACKNOWLEDGEMENTS

We thank Asma Boujtat and Gaetan Herinckx for technical help. We are indebted to Dr. Michael Deghelt, Dr. Seung-Hyun Cho, and Dr. Pauline Leverrier for helpful suggestions and discussions and for providing comments on the manuscript. M.A.W. received support from National Institutes of Health grant R01GM139978. We thank Dr. Tommi White and Dr. Javier Seravalli for assistance with the GroEL-CnoX quantitative interaction studies and Dr. Aron Fenton for discussions about cooperative protein binding. We thank the staff at the VIB-VUB facility for Bio Electron Cryogenic Microscopy (BECM) for assistance in data collection. This work was funded by the Fonds de la Recherche Scientifique (FNRS) grant agreements WELBIO-CR-2015A-03 and WELBIO-CR-2019C-03, the Excellence of Science in Research Program of the FWO and FRS-FNRS (G0G0818N), the Fédération Wallonie-Bruxelles (ARC 17/22-087), GENCI-IDRIS (2021-A0100711524), the Flanders Research Foundation Hercules grant (G0H5916N), the Flanders Research Foundation PhD fellowship program, and the Flanders Institute for Biotechnology – VIB.

REFERENCES

1. Anfinsen CB (1973). Principles that govern the folding of protein chains. Science 181, 223–230. [PubMed: 4124164]
2. Jahn TR, and Radford SE (2005). The Yin and Yang of protein folding. The FEBS journal 272, 5962–5970. [PubMed: 16302961]
3. Ellis RJ (2001). Macromolecular crowding: obvious but underappreciated. Trends in biochemical sciences 26, 597–604. [PubMed: 11590012]
4. Hartl FU, Bracher A, and Hayer-Hartl M (2011). Molecular chaperones in protein folding and proteostasis. Nature 475, 324–332. 10.1038/nature10317. [PubMed: 21776078]
5. Goloubinoff P, Christeller JT, Gatenby AA, and Lorimer GH (1989). Reconstitution of active dimeric ribulose bisphosphate carboxylase from an unfolded state depends on two chaperonin proteins and Mg-ATP. Nature 342, 884–889. [PubMed: 10532860]
6. Horwich AL, and Fenton WA (2020). Chaperonin-assisted protein folding: a chronologue. Quarterly reviews of biophysics 53.
7. Hayer-Hartl M, Bracher A, and Hartl FU (2016). The GroEL–GroES chaperonin machine: a nano-cage for protein folding. Trends in biochemical sciences 41, 62–76. [PubMed: 26422689]
8. Hohn T, Hohn B, Engel A, Wurtz M, and Smith PR (1979). Isolation and characterization of the host protein groE involved in bacteriophage lambda assembly. Journal of molecular biology 129, 359–373. [PubMed: 379349]
9. Hendrix RW (1979). Purification and properties of groE, a host protein involved in bacteriophage assembly. Journal of molecular biology 129, 375–392. [PubMed: 379350]
10. Braig K, Otwinowski Z, Hegde R, Boisvert DC, Joachimiak A, Horwich AL, and Sigler PB (1994). The crystal structure of the bacterial chaperonln GroEL at 2.8 Å. Nature 371, 578–586. [PubMed: 7935790]
11. Chandrasekhar GN, Tilly K, Woolford C, Hendrix R, and Georgopoulos C (1986). Purification and properties of the groES morphogenetic protein of Escherichia coli. Journal of Biological Chemistry 261, 12414–12419. [PubMed: 3017973]
12. Hunt JF, Weaver AJ, Landry SJ, Gierasch L, and Deisenhofer J (1996). The crystal structure of the GroES co-chaperonin at 2.8 Å resolution. Nature 379, 37–45. [PubMed: 8538739]
13. Xu Z, Horwich AL, and Sigler PB (1997). The crystal structure of the asymmetric GroEL–GroES–(ADP) 7 chaperonin complex. Nature 388, 741–750. [PubMed: 9285585]

14. Langer T, Pfeifer G, Martin J, Baumeister W, and Hartl F-U (1992). Chaperonin-mediated protein folding: GroES binds to one end of the GroEL cylinder, which accommodates the protein substrate within its central cavity. The EMBO journal 11, 4757–4765. [PubMed: 1361169]
15. Martin J, Mayhew M, Langer T, and Hartl U (1993). The reaction cycle of GroEL and GroES in chaperonin-assisted protein folding. Nature 366, 228–233. [PubMed: 7901770]
16. Goemans CV, Vertommen D, Agrebi R, and Collet J-F (2018). CnoX is a chaperedoxin: a holdase that protects its substrates from irreversible oxidation. Molecular cell 70, 614–627. e617. [PubMed: 29754824]
17. Goemans CV, Beaufay F, Arts IS, Agrebi R, Vertommen D, and Collet J-F (2018). The chaperone and redox properties of CnoX chaperedoxins are tailored to the proteostatic needs of bacterial species. mBio 9, e01541–01518. [PubMed: 30482828]
18. Lin J, and Wilson MA (2011). Escherichia coli thioredoxin-like protein YbbN contains an atypical tetratricopeptide repeat motif and is a negative regulator of GroEL. Journal of Biological Chemistry 286, 19459–19469. [PubMed: 21498507]
19. Li G-W, B. D, Gross CA, Weissman JS (2014). Quantifying absolute protein synthesis rates reveals principles underlying allocation of cellular resources. . Cell 157, 624–635. [PubMed: 24766808]
20. Weissman JS, Hohl CM, Kovalenko O, Kashi Y, Chen S, Braig K, Saibil HR, Fenton WA, and Norwich AL (1995). Mechanism of GroEL action: productive release of polypeptide from a sequestered position under GroES. Cell 83, 577–587. [PubMed: 7585961]
21. Genevaux P, Keppel F, Schwager F, Langendijk-Genevaux PS, Hartl FU, and Georgopoulos C (2004). In vivo analysis of the overlapping functions of DnaK and trigger factor. EMBO reports 5, 195–200. [PubMed: 14726952]
22. Brinker A, Scheufler C, Von Der Mulbe F, Fleckenstein B, Herrmann C, Jung G, Moarefi I, and Hartl FU (2002). Ligand discrimination by TPR domains. Relevance and selectivity of EEVD-recognition in Hsp70 x Hop x Hsp90 complexes. J Biol Chem 277, 19265–19275. 10.1074/jbc.M109002200. [PubMed: 11877417]
23. Clare DK, Vasishtan D, Stagg S, Quispe J, Farr GW, Topf M, Horwich AL, and Saibil HR (2012). ATP-triggered conformational changes delineate substrate-binding and-folding mechanics of the GroEL chaperonin. Cell 149, 113–123. [PubMed: 22445172]
24. Ewalt KL, Hendrick JP, Houry WA, and Hartl FU (1997). In vivo observation of polypeptide flux through the bacterial chaperonin system. Cell 90, 491–500. [PubMed: 9267029]
25. Imlay JA (2008). Cellular defenses against superoxide and hydrogen peroxide. Annu. Rev. Biochem 77, 755–776. [PubMed: 18173371]
26. Ezraty B, Gennaris A, Barras F, and Collet JF (2017). Oxidative stress, protein damage and repair in bacteria. Nat Rev Microbiol 15, 385–396. 10.1038/nrmicro.2017.26. [PubMed: 28420885]
27. Fujiwara K, Ishihama Y, Nakahigashi K, Soga T, and Taguchi H (2010). A systematic survey of in vivo obligate chaperonin-dependent substrates. EMBO J 29, 1552–1564. 10.1038/emboj.2010.52. [PubMed: 20360681]
28. Chaudhry C, Horwich AL, Brunger AT, and Adams PD (2004). Exploring the structural dynamics of the E. coli chaperonin GroEL using translation-libration-screw crystallographic refinement of intermediate states. Journal of molecular biology 342, 229–245. [PubMed: 15313620]
29. Baba T, Ara T, Hasegawa M, Takai Y, Okumura Y, Baba M, Datsenko KA, Tomita M, Wanner BL, and Mori H (2006). Construction of Escherichia coli K-12 in-frame, single-gene knockout mutants: the Keio collection. Mol Syst Biol 2, 2006 0008. msb4100050 [pii] 10.1038/msb4100050.
30. Cherepanov PP, and Wackernagel W (1995). Gene disruption in Escherichia coli: TcR and KmR cassettes with the option of Flp-catalyzed excision of the antibiotic-resistance determinant. Gene 158, 9–14. [PubMed: 7789817]
31. Consortium, U. (2021). Bateman A, Martin MJ, Orchard S, Magrane M, Agivetova R, Ahmad S, Alpi E, Bowler-Barnett EH, Britto R, et al. UniProt: The universal protein knowledgebase in.
32. Mirdita M, Schütze K, Moriwaki Y, Heo L, Ovchinnikov S, and Steinegger M (2022). ColabFold: making protein folding accessible to all. Nature Methods, 1–4. [PubMed: 35017739]

33. Luo T, Pueyo JM, Wahni K, Yvanoff C, Lazar T, dit Ruys SP, Vertommen D, Ezeriņa D, and Messens J (2021). Thiol-disulphide independent in-cell trapping for the identification of peroxiredoxin 2 interactors. Redox biology 46, 102066. [PubMed: 34340028]
34. Zheng SQ, Palovcak E, Armache J-P, Verba KA, Cheng Y, and Agard DA (2017). MotionCor2: anisotropic correction of beam-induced motion for improved cryo-electron microscopy. Nature methods 14, 331–332. [PubMed: 28250466]
35. Rohou A, and Grigorieff N (2015). CTFFIND4: Fast and accurate defocus estimation from electron micrographs. Journal of structural biology 192, 216–221. [PubMed: 26278980]
36. Wagner T, Merino F, Stabrin M, Moriya T, Antoni C, Apelbaum A, Hagel P, Sitsel O, Raisch T, and Prumbaum D (2019). SPHIRE-crYOLO is a fast and accurate fully automated particle picker for cryo-EM. Commun. Biol 2. Nature Publishing Group.
37. Yang Z, Fang J, Chittuluru J, Asturias FJ, and Penczek PA (2012). Iterative stable alignment and clustering of 2D transmission electron microscope images. Structure 20, 237–247. [PubMed: 22325773]
38. Moriya T, Saur M, Stabrin M, Merino F, Voicu H, Huang Z, Penczek PA, Raunser S, and Gatsogiannis C (2017). High-resolution single particle analysis from electron cryo-microscopy images using SPHIRE. JoVE (Journal of Visualized Experiments), e55448.
39. Zivanov J, Nakane T, Forsberg BO, Kimanius D, Hagen WJ, Lindahl E, and Scheres SH (2018). New tools for automated high-resolution cryo-EM structure determination in RELION-3, elife 7, e42166. [PubMed: 30412051]
40. Terwilliger TC, Ludtke SJ, Read RJ, Adams PD, and Afonine PV (2020). Improvement of cryo-EM maps by density modification. Nature Methods 17, 923–927. [PubMed: 32807957]
41. Pettersen EF, Goddard TD, Huang CC, Couch GS, Greenblatt DM, Meng EC, and Ferrin TE (2004). UCSF Chimera—a visualization system for exploratory research and analysis. Journal of computational chemistry 25, 1605–1612. [PubMed: 15264254]
42. Afonine PV, Poon BK, Read RJ, Sobolev OV, Terwilliger TC, Urzhumtsev A, and Adams PD (2018). Real-space refinement in PHENIX for cryo-EM and crystallography. Acta Crystallographica Section D: Structural Biology 74, 531–544. [PubMed: 29872004]
43. Emsley P, and Cowtan K (2004). Acta Crystallographica, Section D: Biological Crystallography. Acta Crystallographica, Section D: Biological Crystallography 60, 2126–2132. [PubMed: 15572765]
44. Jakobi AJ, Wilmanns M, and Sachse C (2017). Model-based local density sharpening of cryo-EM maps. Elife 6, e27131. [PubMed: 29058676]
45. Burnley T, Palmer CM, and Winn M (2017). Recent developments in the CCP-EM software suite. Acta Crystallographica Section D: Structural Biology 73, 469–477. [PubMed: 28580908]
46. Liebschner D, Afonine PV, Baker ML, Bunkóczi G, Chen VB, Croll TI, Hintze B, Hung L-W, Jain S, and McCoy AJ (2019). Macromolecular structure determination using X-rays, neutrons and electrons: recent developments in Phenix. Acta Crystallographica Section D: Structural Biology 75, 861–877. [PubMed: 31588918]
47. Emsley P, and Cowtan K (2004). Coot: model-building tools for molecular graphics. Acta Crystallogr D Biol Crystallogr 60, 2126–2132. S0907444904019158 [pii] 10.1107/S0907444904019158. [PubMed: 15572765]
48. Schneider CA, Rasband WS, and Eliceiri KW (2012). NIH Image to ImageJ: 25 years of image analysis. Nature methods 9, 671–675. [PubMed: 22930834]

Highlights:

- CnoX is a chaperedoxin that performs a chaperone- and a redox- function
- CnoX binds to the apical domain of the bacterial Hsp60 chaperonin GroEL
- CnoX provides redox quality-control for GroEL substrates
- Proteins sharing structural features with CnoX exist in eukaryotes

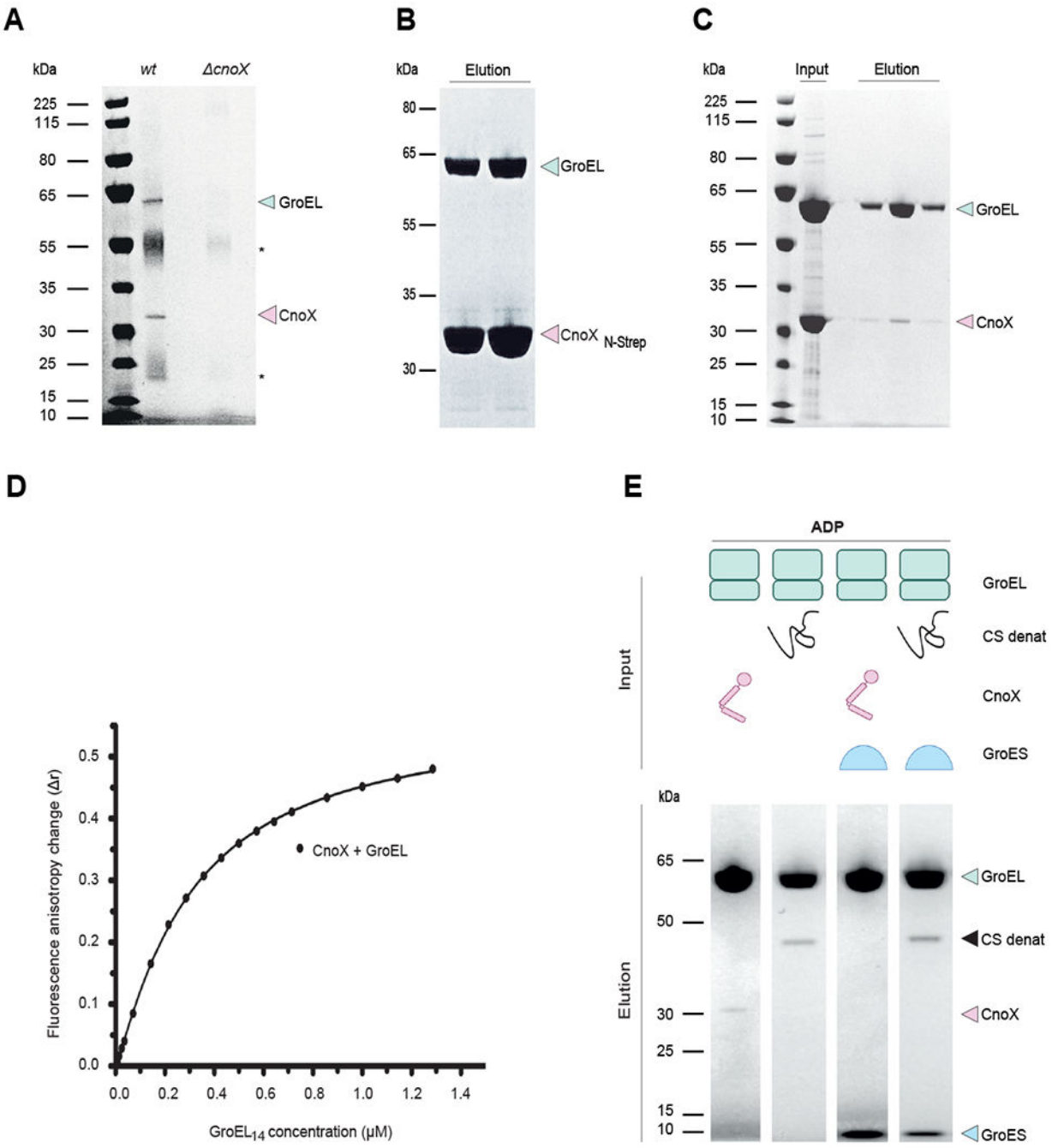

Figure 1. CnoX interacts stably with GroEL.

(A) GroEL co-elutes with CnoX when CnoX is pulled down from wild-type cell extracts using α-CnoX antibodies. Both proteins are absent when the experiment is repeated with extracts prepared from the Δ*cnoX* mutant. The image of sodium dodecyl sulphate–polyacrylamide gel electrophoresis (SDS-PAGE), stained with Coomassie blue, is representative of >3 replicates. * indicates the light and heavy chains of the antibodies. **(B)** Purified $CnoX_{N\text{-}Strep}$ and GroEL form a complex that can be isolated using streptavidin affinity purification. Two fractions are shown.

(C) Purified CnoX and GroEL form a complex that can be isolated using size-exclusion chromatography.

(D) Formation of a complex between FM-CnoX and GroEL can be monitored using fluorescence anisotropy. The noncooperative model gives an adequate fit to these data, with a K_d of 310 ± 10 nM.

(E) CnoX and unfolded CS co-elute with GroEL from a gel filtration column. Addition of GroES triggers the release of CnoX from GroEL, while CS remains bound to GroEL. Size-exclusion chromatography was performed in the presence of ADP (50 μM), and fractions were analyzed by SDS-PAGE. The results are representative of >3 experiments.

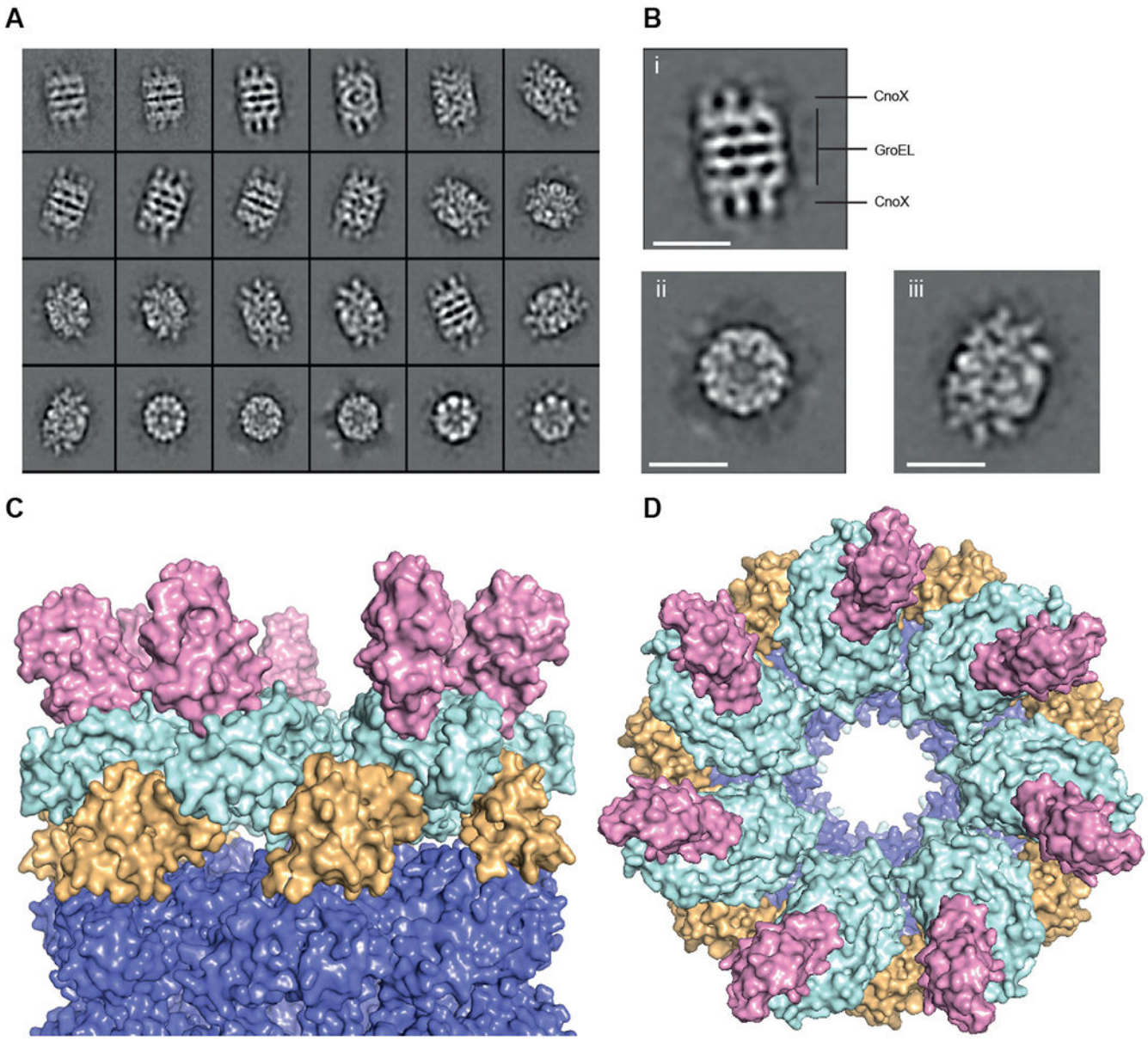

Figure 2. CryoEM shows that the TPR domain of CnoX binds GroEL.

(A, B) CryoEM 2D class averages of the GroEL-CnoX complex reconstituted *in vitro* at a 10:1 molar ratio (scale bar: 100 Å).

(C, D) Side and top view of the structure of the GroEL-CnoX complex shown as a solvent accessible surface. The equatorial, intermediate, and apical domains of GroEL are shown in slate, orange, and light cyan, respectively, and CnoX is shown in pink.

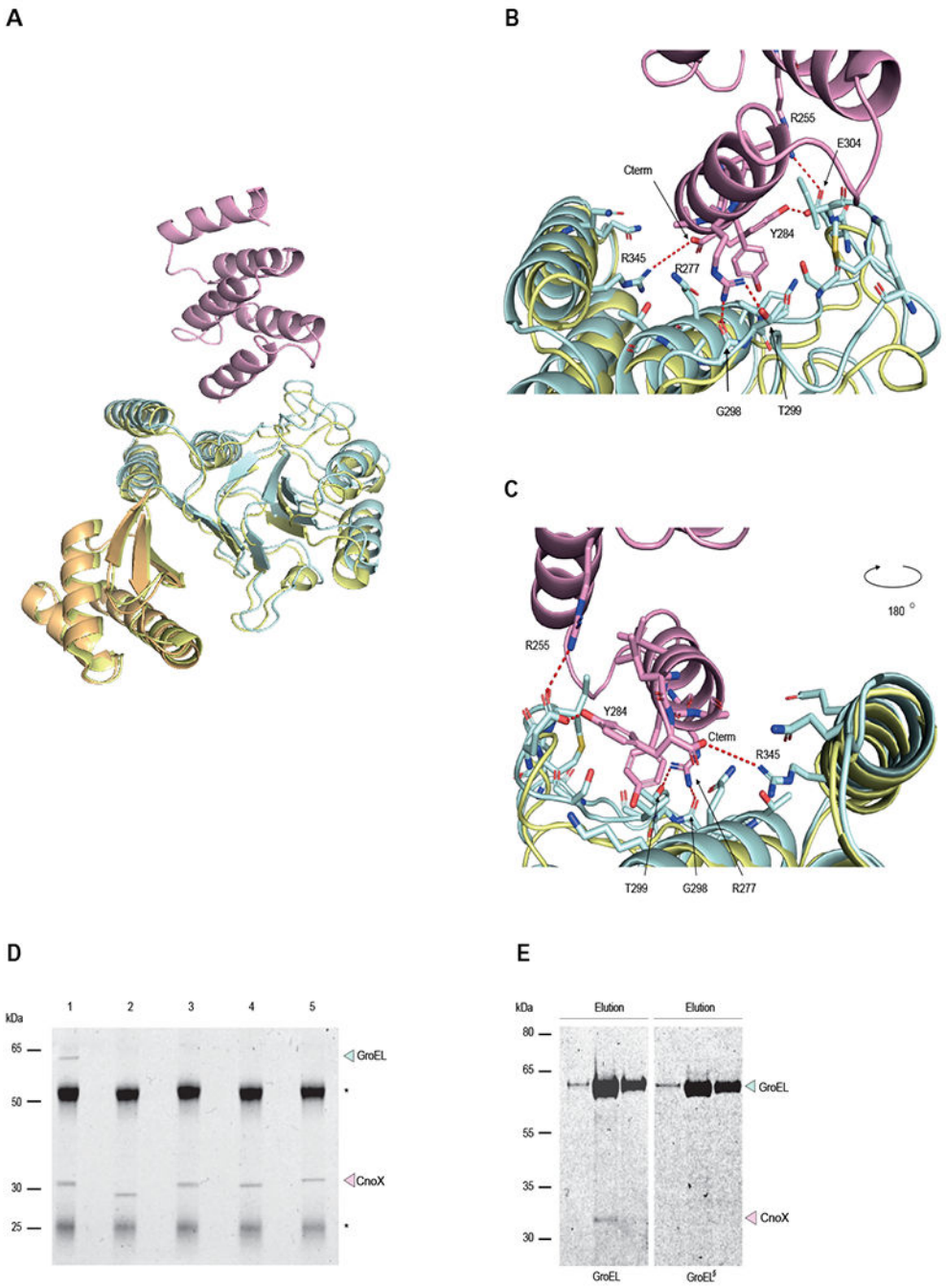

Figure 3. The C-terminal α-helix of CnoX binds a shallow cleft in the apical domain of GroEL.

(A) Ribbon representation of a single GroEL-CnoX protomer. CnoX binds GroEL via its C-terminal α-helix. The intermediate and apical domains of GroEL are shown in orange and light cyan, respectively. CnoX is shown in pink. For comparison, the GroEL-CnoX structure is shown superimposed on the structure of T-state GroEL (yellow; Protein Data Bank [PDB]: 1GRL).

(B, C) Close-up views of the GroEL-CnoX binding interface. CnoX binds GroEL through the following hydrogen-bond and electrostatic interactions (CnoX-GroEL): R255-E304,

R277-G298, R277-T299, Y284-E304, and Y284 C-term-R345. For comparison, the GroEL-CnoX structure is shown superimposed on the structure of T-state GroEL (yellow; PDB: 1GRL).

(D) GroEL co-elutes with CnoX (lane 1) but not with $CnoX_{\Delta Cter}$ (lane 2), $CnoX_{R277L}$ (lane 3), $CnoX_{Y284L}$ (lane 4), or $CnoX_{C\text{-}His}$ (lane 5) when CnoX is pulled down from cell extracts using α-CnoX antibodies. In these experiments, CnoX and its variants were expressed in Δ*cnoX* cells. The SDS-PAGE gel, stained with Coomassie blue, is representative of >3 replicates.

* indicates the light and heavy chains of the antibodies.

(E) $GroEL^{\S}$, a GroEL variant with mutations in the CnoX-binding site (G298A/T299L/V300K/E304L/I305K/M307K/R345L), does not elute together with CnoX from a size-exclusion chromatography column (right), in contrast to wild-type GroEL (left). Three consecutive elution fractions are shown for each chromatography column.

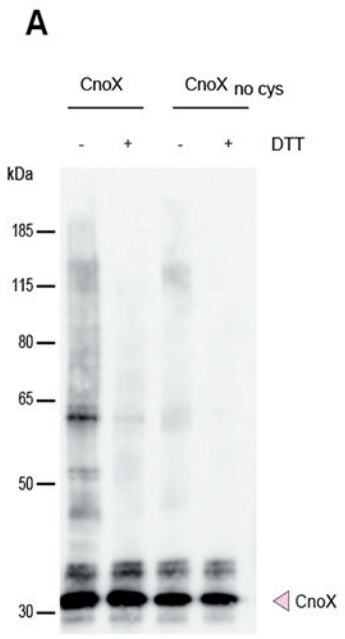

B

Accession #	Protein	Gene
P23908	Acetylornithine deacetylase	argE
P0A6L2	4-hydroxy-tetrahydrodipicolinate synthase	dapA
P0AAI5	3-oxoacyl-[acyl-carrier-protein] synthase 2	fabF
P00370	NADP-specific glutamate dehydrogenase	gdhA
P0ACB2	Delta-aminolevulinic acid dehydratase	hemB
P0A817	S-adenosylmethionine synthase	metK
P0AC41	Succinate dehydrogenase flavoprotein subunit	sdhA
P23721	Phosphoserine aminotransferase	serC
P0AGG8	Metalloprotease TldD	tldD

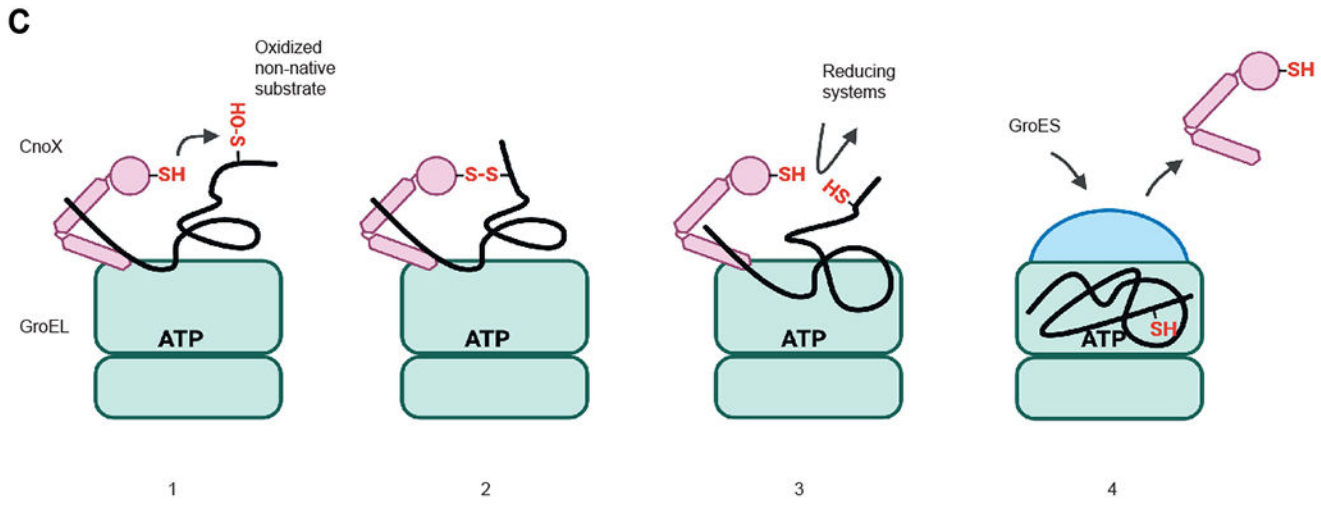

Figure 4. CnoX functions as a molecular plugin to rescue GroEL substrates from oxidative damage.

(A) CnoX co-elutes with GroEL when the chaperonin is pulled down from wild-type cell extracts using specific antibodies. High-molecular-weight complexes corresponding to dithiothreitol (DTT)-sensitive mixed disulfides are detected by α-CnoX antibodies. These complexes are not detected when the experiment is repeated using extracts from cells expressing a CnoX mutant lacking the two cysteine residues, $CnoX_{no\_cys}$.

(B) Obligate GroEL substrates trapped in mixed-disulfide complexes with CnoX and pulled down using α-GroEL antibodies were identified by liquid chromatography with tandem MS (LC-MS/MS).

(C) Model: 1. CnoX forms a stable complex with GroEL via its C-terminal α-helix in a nucleotide-independent manner. Positioned on the apical domain of GroEL, CnoX interacts with incoming substrates for GroEL, acting as a redox quality-control plugin. 2. If the

substrate that reaches GroEL for folding presents oxidized cysteine residues (to a sulfenic acid or in a disulfide bond), CnoX reacts with the substrate via the cysteines of its thioredoxin domain, and a mixed disulfide is formed. Interactions between the substrate and the GroEL cavity occur. 3. Cytoplasmic reducing pathways reduce the mixed disulfide, releasing the substrate in a reduced, folding-competent state. 4. GroES binding triggers CnoX release from GroEL and encapsulation of the substrate within the folding cage for folding.

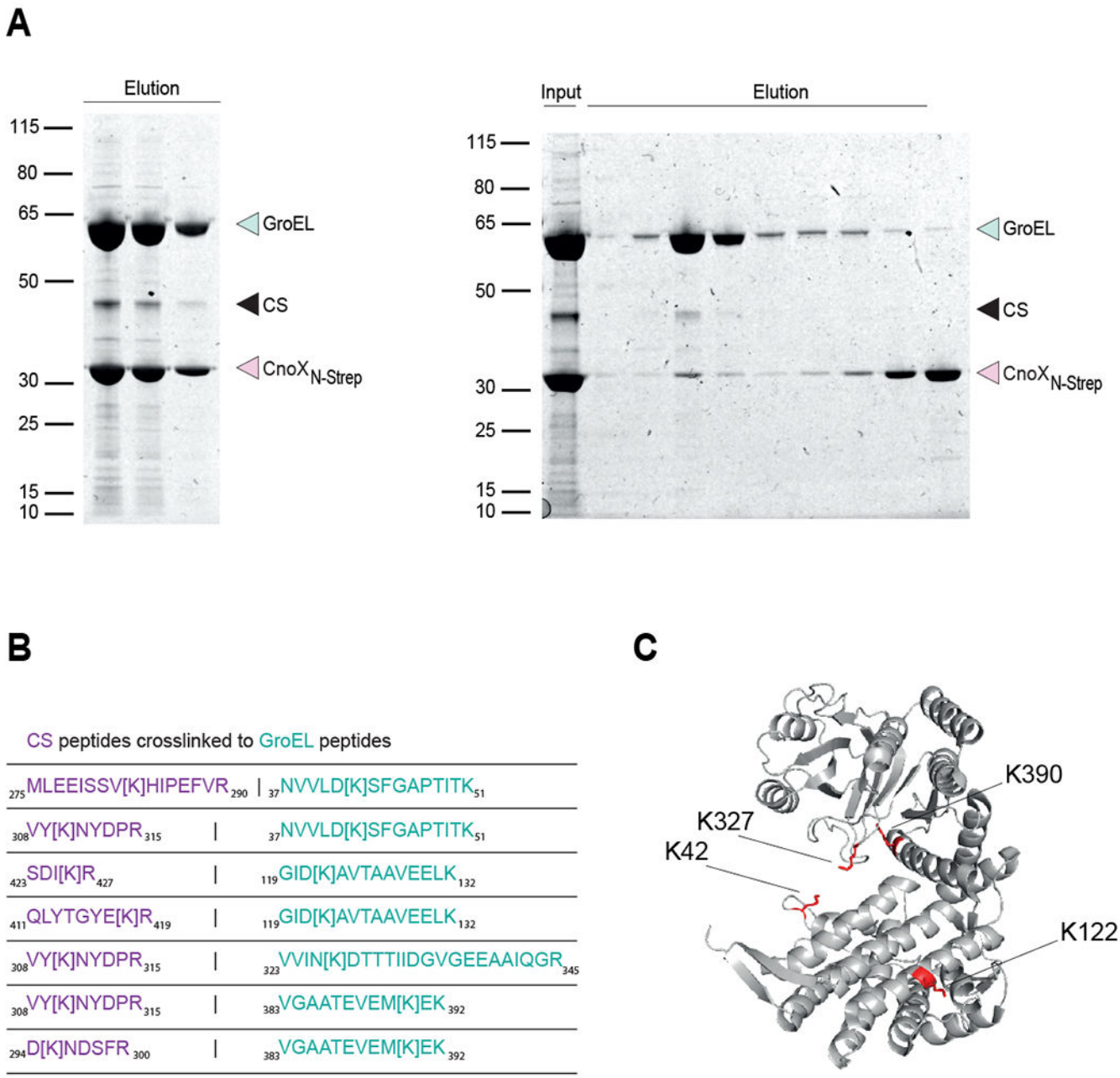

Figure 5. Unfolded CS is present in the cavity of GroEL when in a mixed disulfide with CnoX.

(A) Co-overexpression of $CnoX_{N\text{-}Strep}$, CS, and GroEL leads to the formation of a ternary complex that was purified by affinity chromatography (left) and size-exclusion chromatography (right).

(B) The ternary complex was treated with disuccinimidyl sulfoxide (DSSO) —a crosslinker with an amine-reactive N-hydroxysuccinimide ester at each end of a 7-carbon spacer arm — and subjected to proteolytic digestion with trypsin. The resulting peptide mixture was analyzed by LC-MS/MS. Seven crosslinked peptides between GroEL residues and CS were detected.

(C) Four of the GroEL residues that crosslink to CS face the inside of the cavity.

KEY RESOURCES TABLE

REAGENT or RESOURCE	SOURCE	IDENTIFIER
Antibodies		
Polyclonal rabbit anti-YbbN (CnoX)	CER group, Belgium	Goemans et al., 2018
Polyclonal rabbit anti-GroEL	CER group, Belgium	This study
Anti-rabbit	Sigma	A6154-1ml
Bacterial and virus strains		
E. coli K-12 strain MG1655 (wild type)	JFC lab	N/A
E. coli K-12 strain MC4100	Genevaux lab	N/A
E. coli B strain BL21 (DE3)	JFC lab	N/A
All other strains (Table S3)	This study	This study
Chemicals, peptides, and recombinant proteins		
Ampicillin	Sigma-Aldrich	10835242001
Kanamycin	Sigma-Aldrich	70560-51-9
Chloramphenicol	Sigma-Aldrich	56-75-7
Citrate synthase (CS) from pig hearts	Sigma-Aldrich	C3260
Isopropyl β-D-1-thiogalactopyranoside (IPTG)	Sigma-Aldrich	10724815001
Dithiothreitol (DTT)	Sigma-Aldrich	10197777001
Fluorescein-5-maleimide (FM)	Thermo Fisher	62245
Adenylyl-imidodiphosphate (AMP-PNP)	Sigma-Aldrich	10102547001
Adenosine 5′-diphosphate	Sigma-Aldrich	A2754
Pierce Protein A/G Magnetic Beads	Thermo Fisher	88803
Disuccinimidyl sulfoxide (DSSO)	Thermo Fisher	A33545
ProteaseMAX™ Surfactant	Promega	V2071
Sequencing Grade Modified Trypsin	Promega	V5111
Deposited data		
GroEL-CnoX structure	This study	EMD-14352, PDB: 7YWY
MS-proteomics data	This study and Proteomics Identification Database	N/A
Raw data	Mendeley table	http://dx.doi.org/10.17632/9pt4v7hc93.1
Oligonucleotides		
See Table S5	This study	N/A
Recombinant DNA		
See Table S4	This study	N/A
Software and algorithms		
UCSF Chimera	41	https://www.cgl.ucsf.edu/chimera/
ColabFold	32	N/A
MotionCor2.1	34	N/A
ctffind4.1	35	N/A

REAGENT or RESOURCE	SOURCE	IDENTIFIER
crYOLO 1.5	[36]	N/A
ISAC2	[37]	N/A
RELION3.0	[39]	N/A
phenix.resolve	[40]	N/A
phenix.real.space	[42]	N/A
COOT	[47]	N/A
LocScale	[44]	N/A
CCPEM project package	[45]	N/A
Phenix	[46]	N/A
ImageJ	[48]	N/A
Image Lab	https://www.biorad.com/enbe/product/imagelab-software	N/A